El Said, B., Green, S., & Hallett, S. R. (2014). Kinematic modelling of 3D woven fabric deformation for structural scale features. *Composites Part A: Applied Science and Manufacturing*, *57*, 95-107. https://doi.org/10.1016/j.compositesa.2013.11.006

Kinematic modelling of 3D Woven Fabric Deformation for structural scale features

Bassam El Said*, Steven Green and Stephen R. Hallett

Advanced Composites Centre for Innovation and Science (ACCIS), University of Bristol, Queens Building, University Walk, Bristol, BS8 1TR, United Kingdom.

*Corresponding author:

Email: bassam.elsaid@bristol.ac.uk; telephone: +44 (0) 117 33 15651; fax: + 44 (0) 117 331 5719

Abstract

A multi-scale approach to modelling is optimal for computationally intensive problems of a hierarchical nature such as 3D woven composites. In this paper an approach capable of modelling feature/component scale fabric deformations and defects is proposed. The proposed technique starts with a meso-scale model for predicting the as-woven geometry of a single unit cell using a high fidelity digital element method. The unit cell geometry is then converted into a macro-scale fabric model by geometric reduction then tessellation. On the macro-scale, two and three dimensional approaches to yarn geometry representation are proposed, with an accompanying yarn mechanical model. Each approach is evaluated based on solution accuracy and computational efficiency. The proposed approach is then verified against experimental results on the meso and macro scales. The applicability of this modelling technique to larger scale compaction problems is then investigated. The proposed algorithm was found to be accurate and computationally efficient.

Keywords

A. Fabrics/textiles; B.3-Dimensional reinforcement; C. Weaving; D. Finite element analysis

1-Introduction

Recently, composite materials have seen wide use in many fields including aerospace [1], automotive industry [2], renewable energy [3-5] and civil construction [6]. The introduction of composites in these fields has been driven by its numerous advantages including light weight, relative ease of transportation and assembly, corrosion and fatigue resistance. However, the introduction of these new materials to critical load carrying structures has been hindered by several factors. Among these are the

inherently poor through thickness properties of composites. Conventional composite materials are susceptible to delamination and have poor impact performance [7, 8]. Another factor is the high manufacturing costs of high performance composites. Laying up numerous layers of precisely oriented composites sheets is a time consuming process. Moreover, producing high quality composite components normally involves using expensive pre-preg materials. 3D woven composites is a promising technology which offers a solution to both problems, the poor through thickness properties and the high manufacturing cost of composites.

Conventional 2D composites, whether unidirectional or woven, lack out of plane reinforcement. Hence, through thickness properties are mainly controlled by the matrix. In contrast, 3D woven preforms are made of multiple layers of orthogonal weft and warp yarns with binder yarns woven through thickness. These binder yarns connect some or all the layers together depending on fabric architecture [9, 10]. Due to the load carrying capacity of the through-thickness direction fibres, 3D woven composites exhibit enhanced inter-laminar fracture toughness [7,11] and better impact and energy absorption performance [8, 12] when compared to 2D composites. However, these enhanced properties come at the cost of lower in plane mechanical properties. During the weaving process, warp, weft and binder yarns are mechanically interlocked to form the fabric. A process which involves applying tension and bending to the yarns and has been shown to cause fibre breakage. Research has shown that fibre breakage has an adverse effect on woven composite strength [13]. Another major source of in plane properties degradation in 3D woven composites is the crimp and waviness associated with the presence of binder yarns [14-16] as shown in Figure 1. Consequently, it is essential to understand yarn defects occurring during weaving and manufacturing of 3D woven components in order to accurately predict the mechanical performance of a given component. This knowledge can be used to assess different fabric architectures, component geometries, manufacturing methods and eventually be used to design new 3D woven fabric architectures.

Numerical modelling is a powerful tool for understanding the deformation, kinematic and mechanical behaviour of textile composites. This has been widely applied to 2D woven fabric, for example to model draping characteristics [17]. Modelling approaches employ a dedicated constitutive model

capable of representing the fibrous nature of the fabric. These constitutive models can be applied on the meso scale where each yarn is represented independently in a finite element simulation [18-22]. Additionally, these models can be expanded to represent sheets of woven materials with fibres in multiple directions [23, 24]. 3D woven fabrics introduce an additional level of complexity to the 2D draping process. The existence of out of plane binder yarns introduces out of plane and in plane deformation coupling. Several discrete methods have been developed to model the kinematics of the weaving and /or the compaction process. Of notable interest is the digital element family of models [25-29]. In the digital element technique each yarn is represented by a bundle of 1D element chains connected using frictionless pins. Contact models are used to simulate the beam elements interaction during weaving and/or compaction. A similar approach using beam elements to calculate as-woven geometries is given by Durville [30, 31]. In this approach a dedicated contact algorithm uses fibre disentanglement to represent the weaving process. These types of methods can be reasonably accurate when predicting the fabric deformation on a unit cell scale. Another dedicated approach proposed by Stig et al [32, 33] represents each yarn as a hollow shell. The hollow yarns are inflated by applying internal pressure to find the fabric as-woven state.

Such available modelling techniques are computationally expensive which limits their applicability to the unit cell scale. In practice, deformations occurring in a woven perform during compaction are the result of tool/fabric interactions. Consequently, these deformations are dependent on the tool geometry as well as the fabric architecture. Unit cell models fall short of capturing the tool geometry effects on the compacted fabric which can be of paramount importance for complex components. Hence, the need arises for a simple and computationally efficient modelling technique which can predict fabric deformation at the feature or component scale without compromising accuracy. In order to simultaneously achieve computational efficiency and accuracy, a multi-scale approach combining high and low fidelity techniques is proposed here.

2 -Modelling technique

2.1 –Overview

As discussed in the previous section, components manufactured from woven fabrics can have numerous defects resulting from the weaving and compaction processes. As a result, mechanical and resin flow models built using idealized unit cell geometry will not capture the effect of waviness and crimping which can control the 3D woven composite failure. Despite the recent advances in available computational power, a full mechanical 3D woven fabric model at a structure scale remains unfeasible. An alternative approach is to use multi-scale kinematic models to predict the final deformed fabric geometries at the structural scale. While these models will not provide information regarding the forces, stresses and strains during the weaving and compaction of 3D woven fabrics, kinematic models can provide accurate and detailed internal and external fabric geometries which can be used in turn to build resin infusion and structural scale mechanical models.

The kinematic modelling approach proposed in this paper starts from an accurate geometry of the as-woven unit cell. A meso-scale digital element model implemented in the commercial explicit finite element software LS-Dyna, as proposed by Mahadik et al [29] and further developed by Green et al [34]is used to find the as-woven geometry for the initial unit cell. The input geometry is then tessellated to form a component or feature scale fabric. Next, the full size fabric model is meshed and combined with tooling geometry. The overall contact model is then solved in LS-Dyna to find the deformed fabric geometry using the AUTOMATIC_CONTACT _GENERAL algorithm. This deformed geometry can be later used as an input to other types of modelling such as mechanical and/or resin flow models. The proposed approach is shown schematically in Figure 2.

2.2 – As-woven geometry modelling

In the digital element technique each yarn is represented by a bundle of 1D element chains. Contact models are used to simulate the beam elements interaction during weaving and/or compaction. A digital element model of a single unit cell for the fabric of interest can be used to represent the as woven state of the entire fabric. An initial loose unit cell geometry representing the yarn centreline paths is used to generate a digital element model for a fabric of a given architecture. The diameter of

each beam is calculated based on the number of chains that will be used to model each yarn such that the yarn cross sectional area is preserved. In this paper the number of chains used is 61 per yarn. Higher number of chains significantly increased the model runtime without noticeable effect on results quality [34].

Initially, the yarn paths for warp yarns and weft yarns are assumed to be straight. The location of each yarn is calculated based on the unit cell dimensions, number of yarns per layer and the number of layers of each type. Binder yarn centre line paths are calculated by fitting a cubic spline to the yarn desired path based on the fabric architecture. The spline control points are selected so as to ensure that the binder yarn does not intersect with the warp or weft yarns. Thermal load is then applied to the binder yarns which pull the fabric together forming the desired unit cell as-woven geometry.

In order for the unit cell geometry to remain representative of the fabric after compaction and consequently remain suitable for mechanical modelling, a set of periodic constraints has to be applied to the model. These periodic constraints are applied by connecting yarn end nodes using Multi Point Constraints (MPC), see [34] for details. Figure [3] shows the unit cell weaving simulation starting from the initial loose geometry to the final as woven state.

The generic geometric representation adopted by TexGen [35, 36] has been used to define the yarn surface, as shown in Figure [4]. This geometric representation is quite flexible and is capable of representing yarns of any complex geometry. A conversion process is needed to detect the yarn surfaces which are defined by the multiple chains of elements and convert it to the TexGen geometric representation. This algorithm is required to automatically detect the yarn centreline paths and the cross section points associated with each centreline point. This can be done by carrying out the following steps:

1. The yarn centreline is defined by finding the geometric centre of each group of section points.
2. A set of local coordinates is defined at each centreline point based on the cross-section orientation (see Figure 5a). A geometric plane is defined at this location based on the centreline slope (C) and the vector of cross section maximum width (S) and the centreline point (O) at the location.

3. All the section points are then projected to the section plane defined in the previous step.
4. A section edge detection algorithm is run on the coplanar points resulting from the previous steps. Edge detection is a wide topic in its own right in the field of computer algorithms which cannot be covered in sufficient details here A shrinking rubber band analogy is used for cross-section detection where a fixed number of points is used to define a polygon which conforms to the yarn surface at this given location. An example of the edge detection algorithm being run on a group of random points is shown in Figure 5b. The results of complete yarn detection are shown in Figure 6.
5. While the focus of the unit cell modelling process so far has been to avoid any form of yarn penetration, some minor penetrations might occur as a result of the conversion process. These penetrations can be removed by running the LS-Dyna initial penetration detection step when doing the macro scale modelling which will be discussed in the subsequent sections.

The fabric of choice for analysis in this paper is a 3D woven orthogonal 5 harness satin weave fabric. The warp yarns are 24000 fibres in 8 layers with 2 yarns per layer of the unit cell. The weft yarns are 12000 fibres in 9 layers with 5 yarns per layer of the unit cell. The binders are 6000 fibres each. All fibres are 7 micron diameter carbon fibres. The unit cell size of this fabric is 9.92 mm in weft direction and 27.775 mm in the warp. The as-woven unit cell geometry for this fabric as found by the digital element and converted into TexGen [35, 36] is shown in Figure 7.

2.3 - Yarn modelling for computational efficiency

The digital element method, which was used to find the as-woven geometry in the previous section, represents each yarn in a contact model with bundles of beam elements. The presence of numerous contacts between large numbers of beams is a main reason behind the high computational expense associated with these methods. Here, a simplified representation of the yarns is adopted using a single contact surface built from shell elements for model size reduction and more efficient contact algorithms. However, in order to capture the fabric behaviour with a reduced geometry, special care has to be given to yarn mechanical modelling which will be discussed in sections 2.3 and 2.4. Unit cell geometry found by the digital element approach is typically high resolution where the yarn cross

section is given in detail along the yarn length. In the proposed approach, the yarn contact surface is created by meshing reduced yarn geometry. The reduced geometry can be meshed to form either a 2D yarn cross section or 3D yarn cross section as shown in Figure 4. In a 3D approach shell elements trace the yarn surface giving an accurate representation of the yarn geometry. While in a 2D representation the shell elements represent the yarn mid plane and the shell element thickness is varied to represent the yarn thickness at any given point. The yarn geometric representation used for this paper is the same as adopted by the fabric geometry pre-processor TexGen [35, 36]. In this representation, the yarn centreline path is defined using nodes along the yarn length. At each node, the yarn cross section is defined by a number of section points. For reasons of computational efficiency, a geometric reduction step is needed to reduce the as-woven geometry resolution. Initially, the number of nodes along the yarn centreline is reduced based on the yarn path curvature at each node and a maximum element size. Next, the number of points defining the yarn cross section is reduced at each node. This is done by defining a curvilinear coordinate coinciding with the yarn surface at the section being processed. This local coordinate is then used to interpolate a fixed number of points which will replace the high resolution geometry defining the yarn cross section at this location. At each centreline node, 8 section points are used for 3D representation, while 12 points are used for the 2D representation since this approach involves further geometric reduction. As a final step, the yarn cross section points are offset in the section plane to account for the shell element thickness using a generic polyline curves offset algorithm [37].

2.4 - Three dimensional representations of yarn cross-section

For a 3D representation, points defining the yarn cross section are connected using shell elements to represent the yarn surface. These shell elements will act as contact surfaces during simulation representing the yarn interactions during compaction. However, a yarn kinematic model constructed from hollow shell elements will exhibit unrealistic cross section deformation. Increasing the shell element stiffness by using stiffer material properties or thicker elements will increase the flexural stiffness as well as the in plane stiffness. This will lead to an overall stiff fabric behaviour which is unrealistic. As a result, it is desirable to separate the set of material properties controlling the yarn

cross section deformation and the yarn flexural deformation. This can be achieved by introducing a cross section support at each centreline node. The cross section support fills the yarn cross section at a given point by connecting all the yarn surface nodes using 2D shell elements. The finite element mesh used for kinematic modelling coincides with and is arranged in a similar manner to the yarn geometric representation i.e. all nodes representing the yarn surface are arranged in sections in relation to a yarn centreline points, as given in Figure 4a. Hence, each node on the yarn surface is connected to a yarn cross section. The cross-section supports are meshed using triangular 2D shell elements and assigned visco-elastic material properties. The overall yarn in this representation resembles a monocoque wing structure with the cross-section supports as analogues to ribs .This ensures that the entire yarn deformation is constrained by the internal cross section support. The number of these supports is not selected arbitrarily; it is defined by the number of centreline points used initially to define the yarn geometry. As is the case with any geometric definition, the higher the number of points the more accurate the geometry is described. However, the high resolution comes at the cost of a larger geometric data set and more computational expense when handling the problem. The kinematic aspect of the model will be unaffected by the geometric resolution as long as the resolution is not too low to faithfully describe the problem. For this paper, 8 points were used to define the yarn cross-section at any given location which was chosen as a compromise between geometric accuracy and model runtime.

A typical composite yarn is made of thousands of fibres packed together. During compaction, the individual fibres show no cross section deformation, hence have no contribution to the overall yarn cross section deformation. The cross section deformation is dominated by fibres sliding against each other. For this level of analysis, it is safe to assume that in a woven fabric the yarn cross section deformation can be modelled as shearing deformation as shown in Figure 8 . The shearing deformation effect can be achieved by assigning the yarn cross section support viscoelastic material properties. By choosing a relatively high bulk modulus, the cross section support and hence the entire yarn cross section will exhibit shear dominated deformations. The viscoelastic behaviour of dry fibres

have already been observed and studied in literature [38]. Figure 9 shows a unit cell model meshed using the 3D cross section representation approach.

Since at this stage the yarns are represented as continuous surfaces, we have to make the distinction between two types of fabric volume fractions, an inter-yarn volume fraction and an intra-yarn volume fraction. The inter-yarn volume fraction represents the space contained within the yarn surface as compared to the unit cell volume. The intra-yarn volume fraction represents the volume of fibres contained within each yarn surface as compared to the entire volume contained within this given surface. The meso-scale digital element models from section 2.2 can capture both inter and intra yarn volume fraction variations. However, for the simplified approach, models only capture the inter-yarn volume fraction variation during compaction. The intra-yarn volume fraction is carried over from the digital element model when the single surface was created and remains almost constant at each yarn cross-section because of the shear dominated deformation assumption. This is a reasonable assumption since after the yarns have been interlocked during weaving; minimal change in the intra-yarn volume fraction is expected. It is worth noting that the global volume fraction is dominated by the length of each yarn inside the unit cell boundaries and the inter-yarn spaces. Hence, it will be accurately maintained in both the meso and macro simulation scales.

2.5 - Two dimensional representation of yarn cross-section

The two dimensional approach favours computational speed over accuracy. In this approach, the yarn cross section geometry is reduced to a single contact surface represented by the mid plane. At any given cross section, the geometric reduction process starts by choosing the two most extreme section points as edge points. Then the cross section points are paired together based on the distance from the edge points. For each pair a single finite element node is created at an average location between the two points. The shell element thickness at this point is set to be equal to the distance between the two geometry points. This reduction process and a unit cell mesh using this approach is shown in Figure 10.

For the 2D approach, the cross section deformation during compaction should be represented as a variation in shell element thickness. For LS-Dyna shell elements' thickness change is only as a result of membrane loads. On the other hand, in a real yarn, the cross section deformation is dominated by compression loads acting directly on the yarn surface. Hence, this simplified 2D approach neglects the yarn cross section deformation. Additionally, this approach has the same flexural and in plane stiffness coupling problem discussed in the 3D approach. In order to overcome this issue, the shell elements forming the yarn were reinforced using rod elements along the yarn path. These rods were assigned material properties stiffer than that of the shell elements. Thus, giving the yarn high stiffness in the fibre direction while allowing it to easily shear and bend. The rods are inserted in the LS-Dyna model as 1D elements with only 1 translational degree of freedom at each node. These rods act as a spring linking two subsequent nodes along the yarn length, thus offering the needed additional axial stiffness. The rod cross section area and elastic modulus can be adjusted independently of the 2D shell properties to vary the ratio of bending to in-plane stiffness. Figure 11 shows a 2D yarn surface reinforced by rods.

3 - Unit cell modelling and verification

While, the final goal of this modelling technique it to simulate component / feature scale fabric defects, it is essential to verify that the reduced representation does not have an adverse impact on accuracy. The next section will discuss the construction and calibration of unit cell models against high fidelity models and experimental results. Based on the results the 3D approach was selected to be used for the full scale models

3.1 - Periodic constraints

Due to their hierarchical nature, composite fabrics exhibit periodicity on multiple scales, whether at the micro, meso or macro scale. The scale of interest for this verification exercise is the meso scale unit cell, since the as-woven unit cell geometry is the input to the proposed multi-scale approach. By definition, the unit cell can be used to construct the entire fabric by translation with no need for rotation or reflection [40]. When employing periodic boundary conditions a unit cell model can be used to model the compaction behaviour of an infinite flat fabric [41, 42]. The orthogonal weave

studied in this paper has a unit cell measuring 9.92 mm in weft direction and 27.775 mm in the warp direction. The unit cell is staggered by one yarn in the weft direction when translated to form the entire fabric.

In order for the unit cell geometry to remain representative of the fabric after compaction and consequently remain suitable for mechanical modelling, a set of periodic constraints has to be applied to the model. These periodic constraints are applied by connecting yarn end nodes using Multi Point Constraints (MPC). MPCs connect all degrees of freedom for a yarn tip node to the equivalent node on the opposite side of the unit cell taking offset into consideration. Figure 12 shows how the boundary conditions were applied for the unit cell being studied. To apply consistent periodic constraints, the mesh at the ends of any two yarns being connected must be identical. This condition was included in the meshing algorithm.

3.2 - Unit cell model

A unit cell compaction model was built based on the as-woven geometry for the orthogonal weave from Green et al [34]. Periodic boundary conditions were applied to the model which was compacted between two moving rigid plates. The fabric Volume Fraction (VF) changed from 45% to 56.25% and from a thickness of 7 mm to a thickness of 5.5 mm. Figure 13 shows a comparison between CT scans and digital element results and the proposed models. The results from the unit cell compaction were evaluated based on accuracy and run time. In terms of yarn path and crimp the 3D representation shows good agreement with both experiments and high fidelity models. The 2D model could capture the yarn paths but at the same time fails to capture the correct cross section shape. This failure can be attributed to the lack of yarn cross-section deformation in this representation. The shell elements' cross sections do not deform to accommodate the decrease in unit cell volume under compaction. At higher volume fractions and as the distance between the tool plates gets smaller, the contact algorithm can fail at some locations and hence form localized tool surface penetrations. Additionally, the 2D representation shows large gaps which will become voids or resin rich zones in comparison with the 3D representation and the experimental results. Both observations can be attributed to the lack of cross section deformation which is the main driver of fabric deformation during the compaction

process. From a runtime point of view, the 2D representation was 35% faster than the 3D representation. The reduction in computational load associated with the 2D representation does not however justify the significant loss in accuracy. When comparing the 3D representation to the digital element model a significant reduction in CPU time up to 90% is noticed. Since the number of unit cells is squared as fabric dimensions increases, the runtime reduction will be further amplified for larger fabric models. Hence, the 3D was considered an efficient representation and was selected for use with larger scale models.

3.3 – Model Inputs

For both the 2D and 3D models, the material properties values were selected via several iterations and comparisons with meso-scale digital element models. The proposed modelling technique is a kinematic model where it is more important to capture the deformation of the fabric architecture (e.g. yarn crimp and resin pockets) than the compaction forces. Verification and result assessment is therefore based on the geometric similarities between the experimental geometry and the geometries predicted by the models. The yarn kinematic behaviour is controlled by the volume of fibres in each yarn, the interaction with other yarns at a given location and the interaction with the tool surface. All these factors are independent from the yarn mechanical properties and are fabric architecture properties. Hence, the kinematic modelling with a calibrated set of material properties will be able to predict paths and cross sections accurately. Binder yarns segments which are allowed to move unconstrained inside the fabric will have paths and cross-sections which are more dependent on their mechanical properties. An example is the binder yarns in the orthogonal fabric being studied in this paper. Figure 14 shows the binder yarn paths as predicted by the 3D macro-scale model for four different material properties overlaid on the CT scan results. The comparison shows that the constrained segment (between upper tool and weft yarns) of the binder yarn is matching in all four materials. However, the unconstrained segments show slight differences in terms of yarn cross section and path. This exercise was carried out for various combinations of materials properties to select the best set of material properties to use for the 3D representations. Due to the noticeable differences between the 2D representation results and the CT scan, as well as the penetration occurring in the 2D

model, a similar comparison process could not be carried out effectively for the 2D model. The set of material properties, which were considered optimum after the calibration exercise against the orthogonal fabric CT scans, were used to model a layer to layer interlock fabric. A comparison between the simulation results from the 3D representation, digital element and CT scans are shown in Figure 15. The results were found to be good in agreement with the CT scan models of this second fabric. This reinforces the decision to carry only the 3D tow representation forward to the structural scale.

Two separate material models were used for the 3D representation, an elastic-plastic model for the shell elements representing the yarn surface and a viscoelastic material model [39] for the shell elements forming the yarn cross-section support as discussed in section 2.4. The selection of elasto-plastic model for the yarn surface was based on the physical behaviour of yarns. The physical yarn response will be elastic along fibres axis but in the model bending and transverse compression will induce plastic deformation. In the case of the real yarn, once the fibres slide against each other they do not return to the original configuration without an external pressure, thus there is a permanent "plastic-like" deformation which the model captures, albeit through a different mechanism. A secondary consequence is that there is also plastic deformation in the longitudinal direction, but since in-plane forces on the yarns are small this is likely to be a second order effect

The material properties set selected to be sued for macro modelling corresponds to the results shown Figure 14 a). The yarn surface had a shear modulus of 5 N/mm^2, a tangential modulus of elasticity of 100 N/mm^2 and a bulk modulus of 200 N/mm^2. The yield strength (60 N/mm^2) based on the magnitude of stresses generated during the simulation to allow the yarn surface to yield during compaction. This feature allowed the model to mimic the yarn flexural behaviour since a real yarn response is mostly inelastic. The viscoelastic core material was given an initial shear modulus of 25 N/mm^2 and an infinite shear modulus of 50 N/mm^2 with a decay constant of 0.1 and a bulk modulus 200 N/ mm^2. For the 2D representation, an elastic-plastic material model was used for the shell elements responsible of the yarn flexural response. The rod supports were given a kinematic-plastic material model since the elasto-plastic material model is not available for rod elements in LS-Dyna.

Mass scaling was used in all models to increase solution speed but care was taken to avoid introducing undesirable inertial effect.

4- Feature /component scale modelling and verification

4.1 - Full scale as-woven fabric models by tessellation

Creating a component scale fabric model is achieved by tessellating the as-woven unit cell geometry to form a full scale fabric. This process involves copying the unit cell geometry multiple times until the required size is reached. Next, to maintain mechanical and contact consistency, yarns are merged to similar yarns from the adjacent unit cells to form continuous yarns throughout the fabric. Finally, an equivalence algorithm merges any overlapping geometry points as a result of yarn merging. The tessellation process is a computationally expensive process, requiring handling and processing large amounts of geometry data. The tessellation algorithm used in this paper was inspired by the pyramid based graphic texturing mapping techniques used in computer graphics [43]. In this technique, multiple versions of an image are stored in an array representing a pyramid. The images stored at the pyramid bottom have the highest resolution while the image stored at the top has the lowest resolution. Similarly, during tessellation, a unit cell is copied once then yarns are merged to form a small piece of fabric. Then the resulting geometry is translated again to get a larger fabric with higher resolution. This process is repeated until the desired fabric size is achieved. This approach ensures that at each level the yarn merging is carried out on the unit cell edges only. Figure 16 shows a schematic for the tessellation process and a sample output.

4.2 - Compaction modelling

A major influence on the compaction process is the tool/fabric interaction. In most applications, Liquid resin infusion is the manufacturing process of choice for dry fabric performs. Two types of tooling can be used, either closed mould rigid tools or one sided rigid tooling with a flexible upper tool (vacuum bag). In the case of rigid tooling, it is only necessary to model the tool contact surface which interacts with the fabric [44]. The mould surface geometry is created and meshed before being imported into LS-Dyna. Typically, two tool surfaces are used for compaction. Depending on whether a male or female mould is used for initial preform loading, one of the moulds is fixed and the other is

moved towards it with a prescribed velocity. In this case, both tools are modelled as a rigid shell surfaces.

For the case of one sided rigid tooling, the vacuum bag - preform interaction has an overall more compliant behaviour which needs to be included in the model [45]. The simulation is divided in two phases which are; preform loading and vacuum consolidation. During the preform loading phase, an intermediate rigid tool is used to load the fabric and the vacuum bag over the rigid tool. The intermediate tool represents the fabric being loaded into position by hand. This intermediate tool is stopped when the distance between it and the other rigid tool is equal to the as-woven fabric thickness. In the next phase, pressure is applied to the vacuum bag surface to simulate vacuum consolidation. The vacuum bag in these simulations is modelled using shell elements with isotropic elastic material properties. Figure 17 shows a setup for a vacuum compaction model and a final model result.

Several factors contribute to the final solution quality, including the presence of friction. The yarns in the real fabric are usually treated which gives a form of viscous friction between yarns. Hence, viscous friction has to be included in the model or otherwise the fabric will behave loosely and disintegrate during simulation. The static friction coefficient for the LS-Dyna contact algorithm [39] was set to 0.9 and the dynamic friction coefficient to 0.85 which are relatively high values, thus representing the yarn surface treatment. Another important factor is the tool advance speed. A reasonable speed is essential for realistic simulation results. If the tool is moving too fast it will create unrealistic localized fabric defects. Also, at higher tool speeds, the contact algorithm might fail and cause an unstable solution.

4.3 - Full scale models verification

The “humpback bridge” specimen is one which has been designed for determining composites through-thickness tensile strength [46]. Several such test samples had been previously prepared from the same orthogonal fabric described earlier in this paper. Dry preforms were laid on a rigid tool and enclosed in a vacuum bag. The samples were then infused with liquid epoxy resin and cured. The cured composite was cut into 12 mm wide strips samples. Selected samples were CT scanned to show

the internal fibre architecture. Figure 18 shows the tooling dimensions and a final sample. The compaction process of a sample, without any consideration of the resin infusion, was modelled using the vacuum bag compaction approach described in section 4.2. The model run time was 18 hours on a Linux cluster running on 8 cores. A comparison between the CT scan results and the simulation is shown in Figure 19. The model was found to be in good agreement with the experimental results. The yarn paths match those found in the CT scan. Additionally, gaps between yarns in the model correspond well to the resin pockets in the CT scan. Marker 1 on Figure 19 points to the gap formed as a result of the binder yarn interaction with the tool apex while marker 2 points to the gap forming around the tool corners. The gaps shown in the simulation are in good agreement with the experimental results. Marker 3 points to weft yarns overlap as a result of the interaction with each other and with vacuum bag which was also in good agreement with the CT scan. One of the common challenges with vacuum bag manufacturing is thickness variability especially around corners. Figure 20 shows the relative thickness variation along the sample length as predicted by the model in comparison to the experimental results. Both the model and the experiment showed the general trend of the sample being thicker around the corner and thin at the apex but the CT scan showed overall slightly higher thickness variability.

5-Applications to Design for manufacturing

Unlike conventional materials, composite material properties are determined during the component manufacturing process. Consequently, composite materials properties can suffer significant degradation from defects which arise during compaction. The proposed modelling approach offers a tool which can be used by engineers to assess tooling and preform design by identifying the defects and high deformations.

For demonstration purposes a dome component was selected to be modelled. The dome forming problem has been widely addressed in literature for 2D fabrics with several analytical and experimental results available [19, 23, 44, 47-51]. A fabric model with an in-plane dimension of 360 mm in the warp direction and 300 mm in the weft direction was built. The fabric was laid in contact with a female tool with a fabric guide on top. A spherical indenter was used to form the fabric into the

female tool cavity. The indenter has a radius of 72 mm and the cavity has a radius of 77 mm. The fabric guide and tools were modelled as rigid shells. Figure 21 shows the tool geometry. The model run time was 180 hours on 24 cores of an HPC Linux cluster. The analysis offered a detailed view of the compaction where the through-thickness deformation at each location is described in detail while the global fabric behaviour is still captured. Figure 22 shows the deformed fabric model. The fabric edge deformation shown is consistent with dome compaction results for 0^o-90^o 2D fabric given in references [19, 44]. Figure 23 shows the yarn paths on the dome inside and through thickness cross sections at a selected location. The results show that the tool fabric interaction has affected the yarn paths, waviness and crimp at each location differently. While the initial unit cell geometry is constant throughout the fabric, the deformed fabric shows significant variation in unit cell geometry between locations. When loaded, the damage will initiate at the developed weak points within the structure. Hence, failure modelling for complex 3D woven components should take into consideration the compacted fabric architecture.

Such analyses will obviously require more complete validation against physical test data, but this model has served to show here that analysis on a suitably large and complex part is feasible in achievable run times and gives credible results.

6 – Conclusion and discussion

A multi-scale approach to kinematic modelling 3D woven fabric deformations and defects has been proposed. Initial as-woven geometry has been predicted from a meso-scale unit cell digital element model and then used to form a macro-scale shell element model. For the macro-scale model two and three dimensional yarn cross section representations have been studied with different yarn mechanical models. The results from both approaches were verified against experimental results for unit cell compaction. The comparison between the simulations and experimental has shown that yarn cross section deformation dominates the fabric behaviour during compaction. Hence, the three dimensional representation proved to be a good balance between accuracy and computational efficiency.

Feature scale simulations were built and validated against experimental results. These simulations showed good ability to model yarn paths, crimping and voids/resin pockets. A further larger scale

model was built to assess the feasibility of applying this modelling approach to more complex simulations. The results demonstrated a good potential for using the proposed technique to design 3D woven fabric and geometry for manufacturability. The complex features captured by the simulation and experimental results show that the internal fabric architecture of compacted 3D woven composites is affected by the both the initial unit cell architecture as well as the tool geometry. Additionally, in the case of vacuum bag curing, tool mechanical behaviour can be important as well. Hence, including these effects in fabric compaction modelling is necessary for the accurate prediction of 3D woven fabric deformation.

The proposed modelling approach has been applied to a 3D woven orthogonal fabric and a 3D woven layer to layer interlock fabric with good results for both type of fabric as compared to CT scans. Additionally, since the proposed model is primarily kinematic, in theory, it should be applicable to any 3D woven fabric architecture regardless of the fibre type. However, the model inputs selection process discussed in section 3.3 has been carried out specifically for the carbon fibre yarn types used in the experimental validation. It is not clear what kind of errors will be introduced to the model if different types of fibres such as aramid or glass were used and what effects such errors will have on the final mechanical properties of the 3D woven composite component. The macro scale model is quite generic and should be applicable to fabrics types other than 3D woven. The digital element approach used for the meso-scale modelling uses binder yarns to compact the fabric. The absence of these binder yarns in other fabrics types means that this approach will need some adaptation to be applied to other fabric types. For example by applying the thermal load to stitching in the case of multi-axial non crimp fabrics or applying the loads directly to the warp yarns in the case of simple 2D woven materials which is part of on-going work. Finally, the use of meso-scale digital element unit cell geometry as input to the tessellation and the macro-scale models is not limited to digital element models. Any high fidelity source such as CT-scans will suffice so long as the geometry can be clearly identified and digitised.

Acknowledgments

The authors wish to acknowledge the support of Rolls-Royce plc. through the Composites University Technology Centre of the University of Bristol and the Engineering and Physical Sciences Research Council (EPSRC) through the ACCIS DTC.

References

1. Mangalgiri PD. Composite materials for aerospace applications. Bulletin of Materials Science 1999; 22: 657-664.
2. Zhang J, Chaisombat K, He S, Wang CH. Hybrid composite laminates reinforced with glass/carbon woven fabrics for lightweight load bearing structures, Materials and Design 2012;36: 75PE0
3. Ackermann T and Söder L. Wind energy technology and current status: A review. Renewable and sustainable energy reviews 2000; 4(4):315-374.
4. Joselin Herbert GM, Iniyan S, Sreevalsan E and Rajapandian S. A review of wind energy technologies. Renewable and Sustainable Energy Reviews 2007; 11(6): 1117-1145.
5. Marsh G. Wave and tidal power—an emerging new market for composites. Reinforced Plastics 2009; 53(5): 20-24.
6. Hollaway LC. A review of the present and future utilisation of frp composites in the civil infrastructure with reference to their important in-service properties. Construction and Building Materials 2010; 24(12): 2419-2445.
7. Guénon VA, Chou TW and Gillespie JW. Toughness properties of a three-dimensional carbon-epoxy composite. Journal of materials science 1989; 24(11): 4168-4175.
8. Brandt J, Drechsler K and Arendts FJ. Mechanical performance of composites based on various three-dimensional woven-fibre preforms. Composites Science and Technology 1996; 56(3):381-386.

9. Kamiya R, Cheeseman BA, Popper P and Chou TW. Some recent advances in the fabrication and design of three-dimensional textile preforms: A review. Composites science and technology 2000; 60(1):33-47.

10. Mouritz AP, Bannister MK, Falzon PJ and Leong KH. Review of applications for advanced three-dimensional fibre textile composites. Composites Part A: Applied Science and Manufacturing. 1999; 30(12): 1445-1461.

11. Chou S, Chen HC and Chen HE. Effect of weave structure on mechanical fracture behaviour of three-dimensional carbon fiber fabric reinforced epoxy resin composites. Composites science and technology 1992; 45(1): 23-35.

12. Baucom JN and Zikry MA. Evolution of failure mechanisms in 2d and 3d woven composite systems under quasi-static perforation. Journal of composite materials 2003; 37(18):1651-1674.

13. Lee L, Redo-Clark S, Mouritz AP, Bannister MK and Herszberg I. Effect of weaving damage on the tensile properties of three-dimensional woven composites. Composite structures 2002; 57(1): 405-413.

14. Cox BN, Dadkhah MS, Morris WL and Flintoff JG. Failure mechanisms of 3d woven composites in tension, compression, and bending. Acta metallurgica et materialia 1994; 42(12): 3967-3984.

15. Lee B, Leong KH and Herszberg I. Effect of weaving on the tensile properties of carbon fibre tows and woven composites. Journal of reinforced plastics and composites 2001; 20(8):652-670.

16. Mahadik Y and Hallett SR. Effect of fabric compaction and yarn waviness on 3d woven composite compressive properties. Composites Part A 2011; 42(11): 1592-1600.

17. Tan P, Tong L and Steven GP. Modelling for predicting the mechanical properties of textile composites—a review. Composites Part A 1997; 28(11): 903-922.

18. Charmetant A, Vidal-Sall E and Boisse P. Hyperelastic modelling for mesoscopic analyses of composite reinforcements. Composites Science and Technology 2011; 71(14): 1623-1631.

19. Badel P, Vidal-Sall E and Boisse P. Large deformation analysis of fibrous materials using rate constitutive equations. Computers & Structures 2008; 86(11): 1164-1175.

20. Hivet G and Boisse P. Consistent mesoscopic mechanical behaviour model for woven composite reinforcements in biaxial tension. Composites Part B: Engineering 2008; 39(2): 345-361.

21. Lin H, Sherburn M, Crookston J, Long AC, Clifford MJ and Jones IA. Finite element modelling of fabric compression. Modelling and Simulation in Materials Science and Engineering 2008; 16(3).

22. Lin H, Clifford MJ, Long AC and Sherburn M. Finite element modelling of fabric shear. Modelling and Simulation in Materials Science and Engineering 2008; 17(1).

23. Badel P, Gauthier S, Vidal-Sall E and Boisse P. Rate constitutive equations for computational analyses of textile composite reinforcement mechanical behaviour during forming. Composites Part A: Applied Science and Manufacturing 2009; 40(8): 997-1007.

24. Khan MA, Mabrouki T, Vidal-Salle E and Boisse P. Numerical and experimental analyses of woven composite reinforcement forming using hypoelastic behaviour. Application to the double dome benchmark. Journal of Materials Processing Technology 2010; 210(2):378-388.

25. Wang Y and Sun X. Digital-element simulation of textile processes. Composites science and technology 2001; 61(2):311-319.

26. Wang Y, Miao Y, Swenson D, Cheeseman BA, Yen CF and LaMattina B. Digital element approach for simulating impact and penetration of textiles. International Journal of Impact Engineering 2010; 37(5): 552-560.

27. Zhou G, Sun X and Wang Y. Multi-chain digital element analysis in textile mechanics. Composites science and Technology 2004; 64(2):239-244.

28. Sun X and Sun C. Mechanical properties of three-dimensional braided composites. Composite structures 2004; 65(3): 485-492.

29. Mahadik Y and Hallett SR. Finite element modelling of tow geometry in 3D woven fabrics. Composites Part A: Applied Science and Manufacturing 2010; 41(9):1192-1200.

30. Durville D. Finite element simulation of textile materials at mesoscopic scale. Finite element modelling of textiles and textile composites, St-Petersburg, 26-28 September 2007.

31. Durville D. Simulation of the mechanical behaviour of woven fabrics at the scale of fibres. International journal of material forming 2010; 3:1241-1251.

32. Stig F and Hallström S. Spatial modelling of 3d-woven textiles. Composite Structures 2012; 94(5):1495-1502.

33. Stig F and Hallström S. A modelling framework for composites containing 3d reinforcement. Composite Structures 2012; 94(9):2895-2901.

34. Green S, Long AC, El Said BSF and Hallett SR. Numerical modelling of 3D woven preform deformations. Composites Structures 2013, In press.

35. Sherburn M, Robitaille F, Long A, and Rudd C. Geometric pre-processor for the calculation of physical properties of textiles. In: Proceedings of the Industrial Simulation Conference, Malaga, Spain, 2004, p. 479–486

36. Sherburn M. Geometric and mechanical modelling of textiles. Doctor of Philosophy: University of Nottingham, July 2007.

37. Liu XZ, Yong JH, Zheng GQ and Sun JG. An offset algorithm for polyline curves. Computers in Industry 200758(3): 240-254.

38. Bickerton S, Buntain MJ and Somashekar AA. The viscoelastic compression behavior of liquid composite molding preforms. Composites Part A: Applied Science and Manufacturing 2003;34(5): 431-444.

39. Hallquist JO. LS-DYNA theory manual. Livermore Software Technology Corporation 2006.

40. Cox BN and Flanagan G. Handbook of analytical methods for textile composites. National Aeronautics and Space Administration 1997; 4750.

41. Li S, Warrior N, Zou Z and Almaskari F. A unit cell for FE analysis of materials with the microstructure of a staggered pattern. Composites Part A 2011; 42(7):801-811.

42. Tang X and Whitcomb JD. General techniques for exploiting periodicity and symmetries in micromechanics analysis of textile composites. Journal of composite materials 2003; 37(13):1167-1189.

43. Adel son EH, Anderson CH, Bergen JR, Burt PJ and Ogden JM, Pyramid methods in image processing. RCA engineer 1984; 29(6): 33-41.

44. Gelin JC, Cherouat A, Boisse P and Sabhi H. Manufacture of thin composite structures by the rtm process: Numerical simulation of the shaping operation. Composites science and technology1996; 56(7): 711-718.

45. Kang MK, Lee WI and Hahn HT. Analysis of vacuum bag resin transfer molding process. Composites Part A: Applied Science and Manufacturing 2001; 32(11): 1553-1560.

46. Wisnom MR, Jones MI, Size effects in interlaminar tensile and shear strength of unidirectional glass fibre-epoxy**.** Journal of Reinforced Plastics and Composites 1996; 15: 2–15.

47. Skordos AA, Sutcliffe MP, Stochastic simulation of woven composites forming. Composites Science and Technology 2008; 68(1): 283-296.

48. Cherouat, A, Billoët, JL, Mechanical and numerical modelling of composite manufacturing processes deep-drawing and laying-up of thin pre-impregnated woven fabrics. Journal of materials processing technology 2001; 118(1): 460-471.

49. Hamila N, Boisse P, Simulations of textile composite reinforcement draping using a new semi-discrete three node finite element. Composites Part B: Engineering 2008; 39(6):999-1010.

50. Boisse P, Cherouat A, Gelin JC, Sabhi H. Experimental study and finite element simulation of a glass fiber fabric shaping process. Polymer composites 1995; 16(1): 83-95.

51. Dong L, Lekakou C, Bader MG, and Processing of composites: simulations of the draping of fabrics with updated material behaviour law. Journal of Composite Materials 2001; 35(2):138-163.

Figure 1. *Schematic of the deformation of a warp and weft yarns near a binder yarn crossover.*

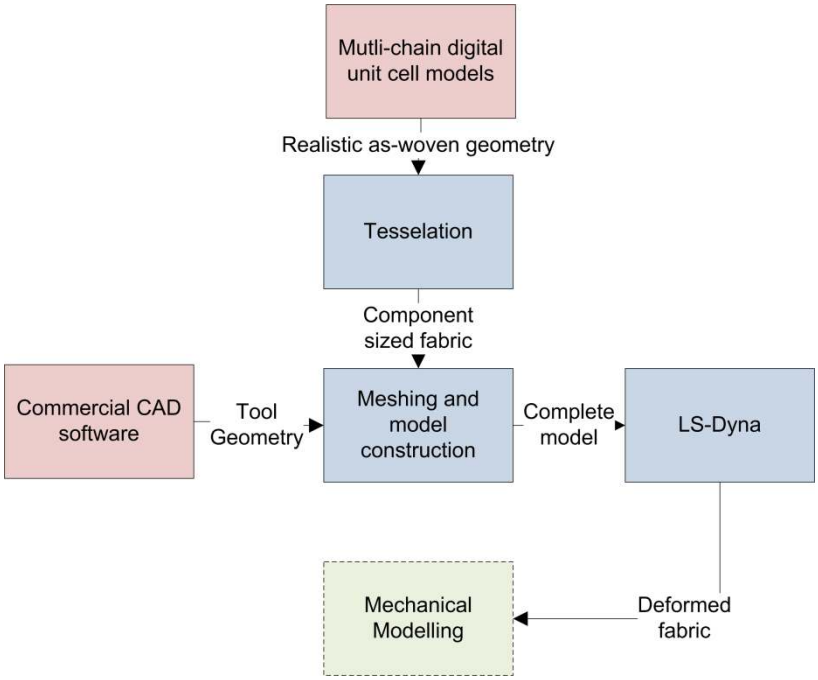

Figure 2. *Proposed modelling techniques schematic.*

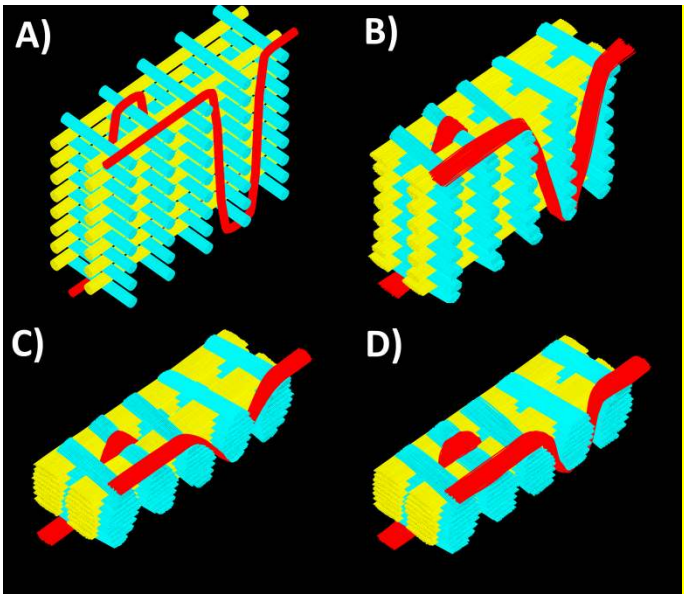

Figure 3. *Digital element model results a) initial geometry b) thermal load applied c) as-woven thickness reached d) final compacted unit cell geometry (tool not displayed).*

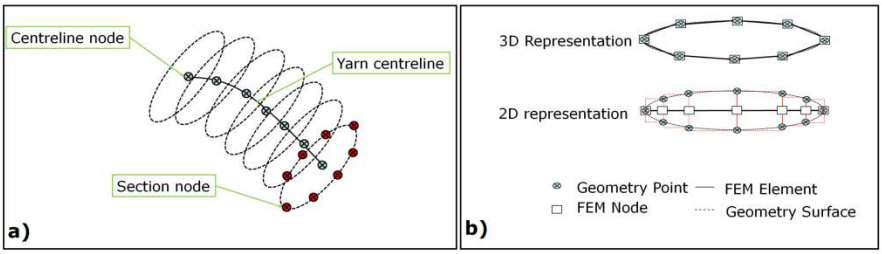

Figure 4. *a) Yarn geometry representation: b) yarn cross section representation.*

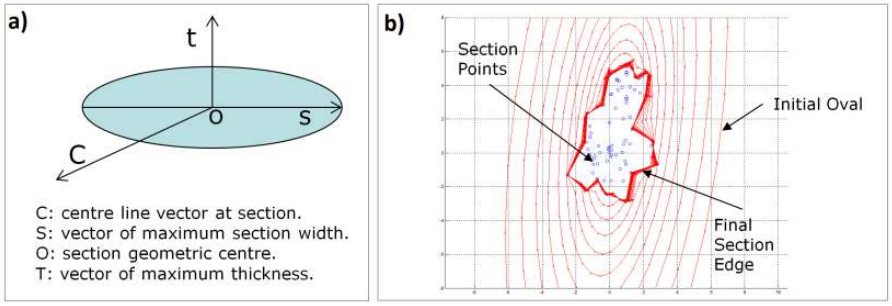

Figure 5. *a) Yarn cross-section local axis definition b) Cross-Section edge detection applied to a set of random points*

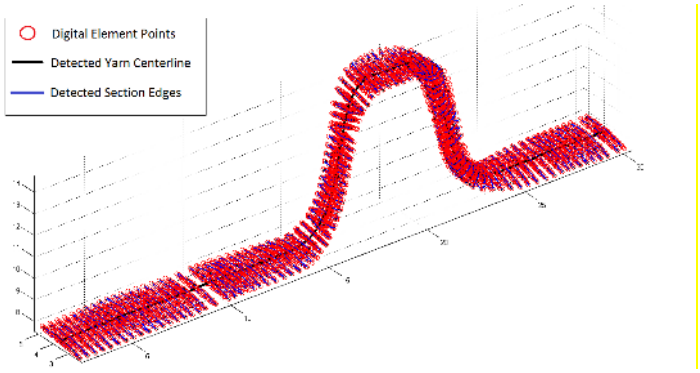

Figure 6. *The yarn conversion algorithm applied to a binder yarn*

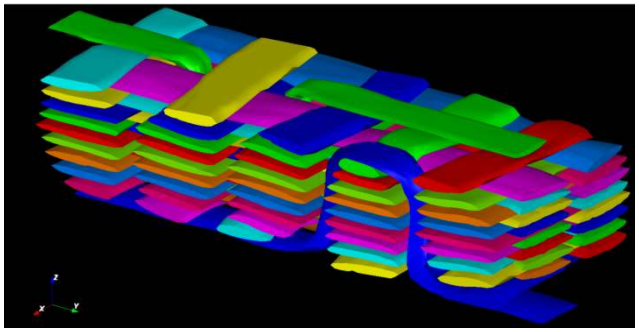

Figure 7*. Realistic as woven geometry computed using a digital element method imported into the TexGen geometric pre-processor [35, 36].*

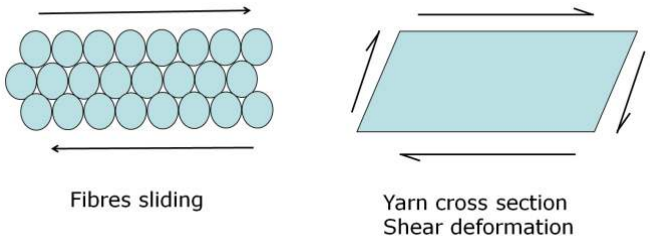

Figure 8. *Shear deformation representation of yarn cross section deformation.*

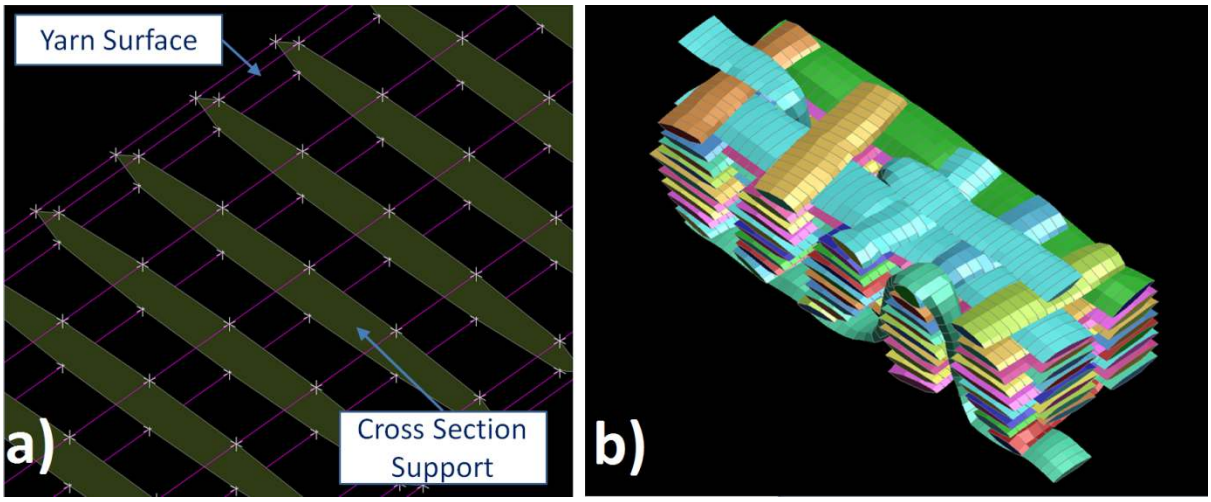

Figure 9. *Mesh for 3D yarn representation: a) One yarn surface is plotted as wireframe to show the cross section supports, b) Uncompacted unit cell model.*

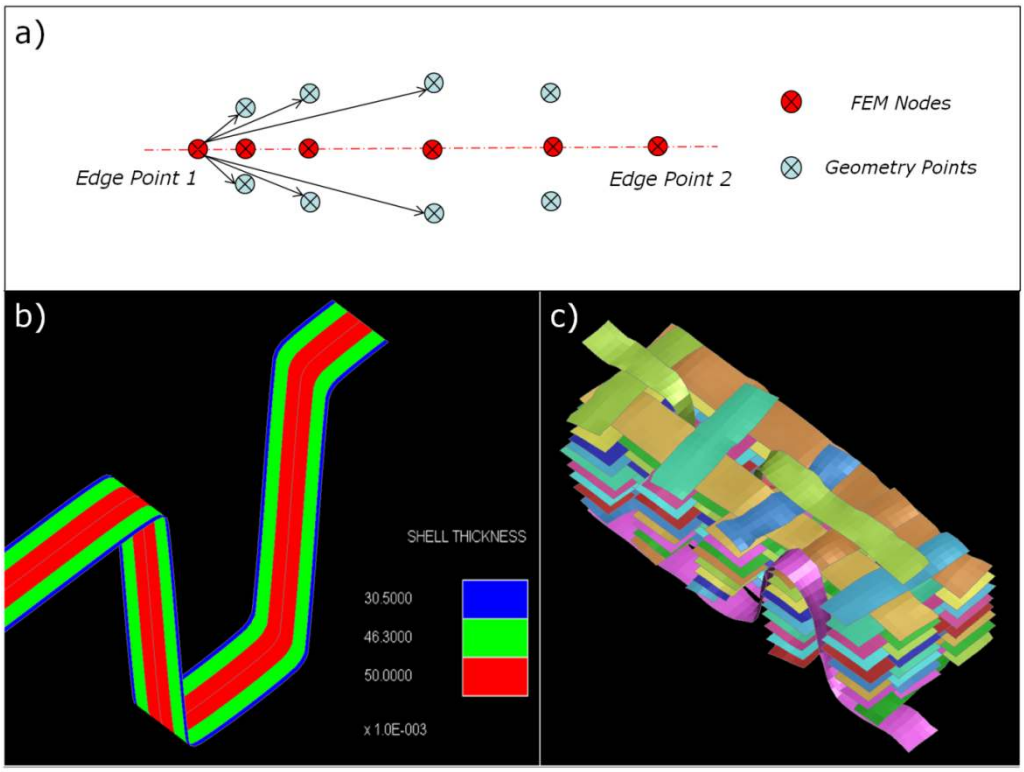

Figure 10. *Mesh for 2D yarn representation: a) Schematic of the reduction algorithm, b) Contour plot of thickness distribution on a yarn with an oval cross section c) Uncompacted unit cell model.*

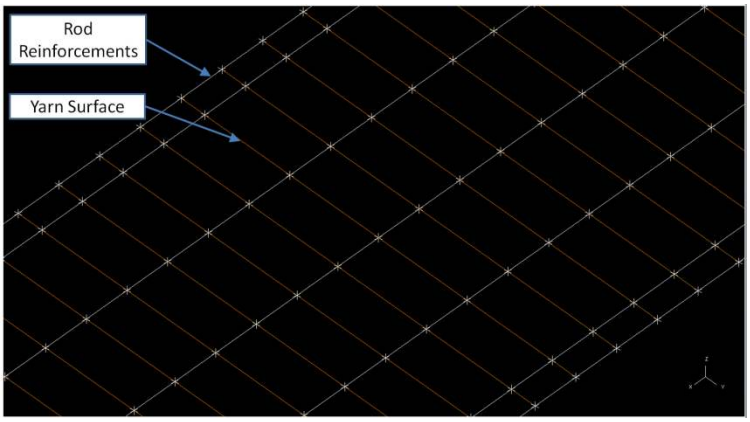

Figure 11. *2D yarn representation, the yarn is plotted in wire frame to show the rod reinforcements (shown in white).*

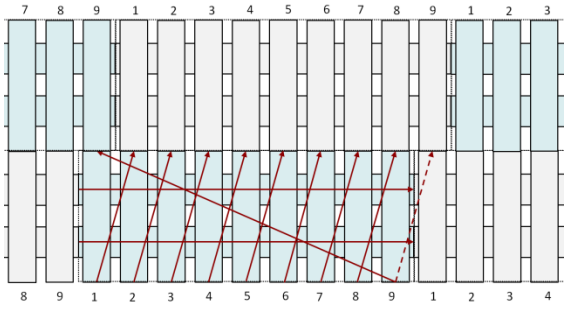

Figure 12. *A schematic of the fabric unit cells showing the periodic constraints in both the warp and weft direction.*

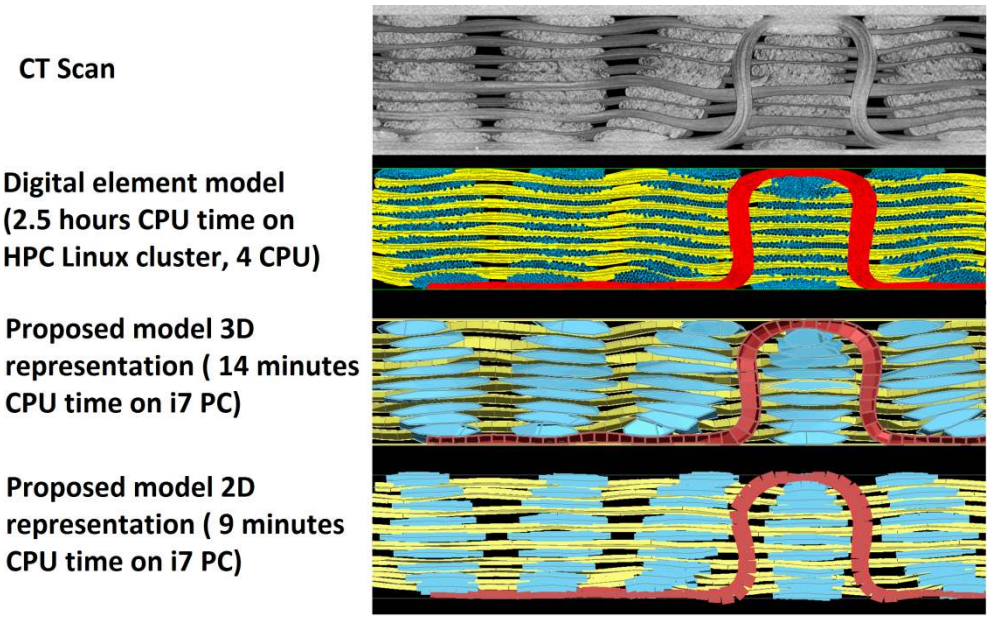

Figure 13. *Unit cell model compaction results.*

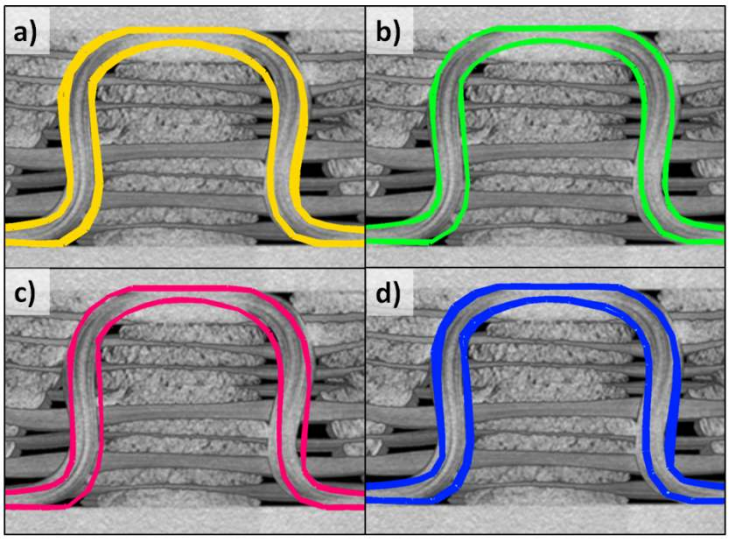

* Material properties	A	B	C	D
Surface shear modulus (N/mm^2)	5	10	10	5
Surface tangential modulus of elasticity (N/mm^2)	100	500	100	100
Surface bulk modulus (N/mm^2)	200	600	200	200
Yield strength (N/mm^2)	60	60	60	60
Core initial shear modulus (N/mm^2)	50	10	10	5
Core infinite shear modulus (N/mm^2)	25	5	5	2.5
Core bulk modulus (N/mm^2)	200	200	300	300
Core decay constant	0.1	0.1	0.1	0.1

Figure 14. *Detailed comparison for binder yarn path and deformation as compared to the CT –Scan for four different material types. (The material properties shwon her is only a subset of those tested)*

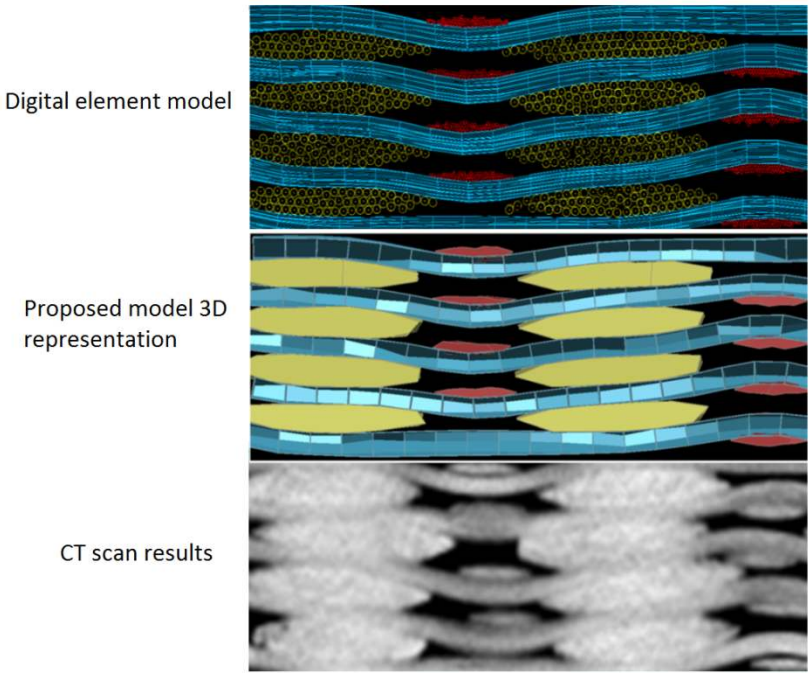

Figure 15. *Compaction results for a layer to layer interlock fabric*

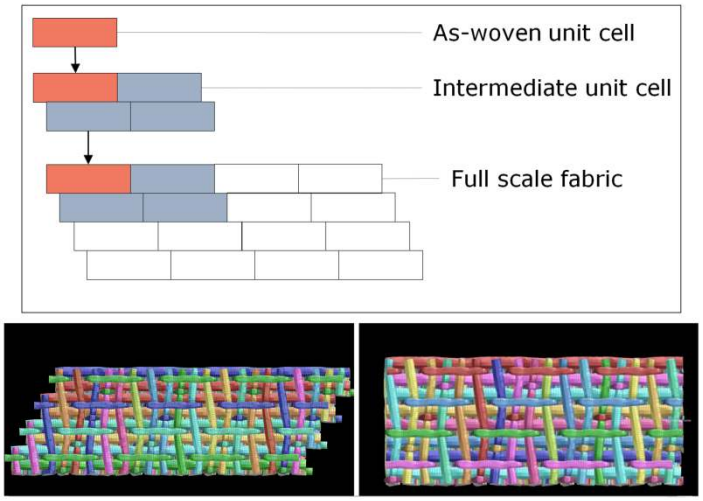

Figure 16. *a) Tessellation algorithm schematic, b) 4X4 unit cells fabric model, c) fabric model trimmed to a rectangular region.*

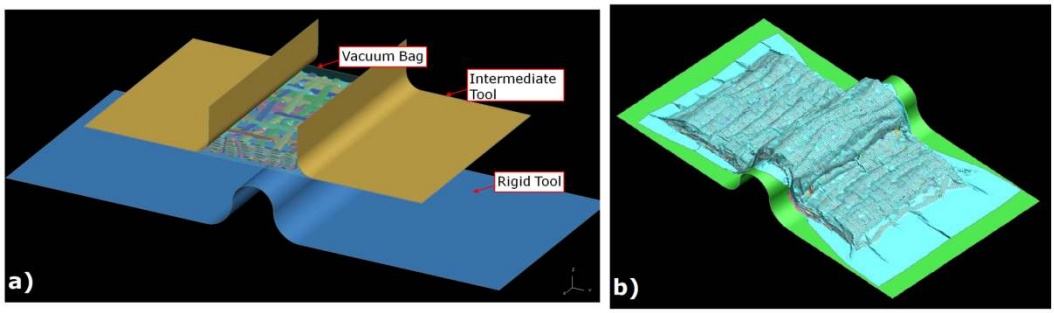

Figure 17. *Vacuum compaction model: a) model setup, b) final result.*

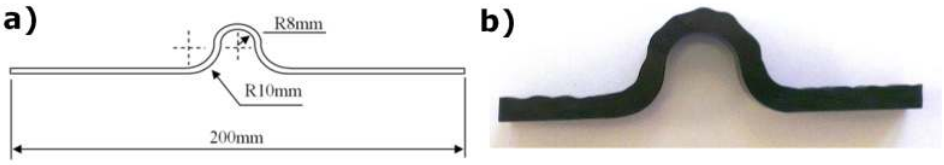

Figure 18. *a) Sketch of rigid tool used in sample: b) central section of a cured sample.*

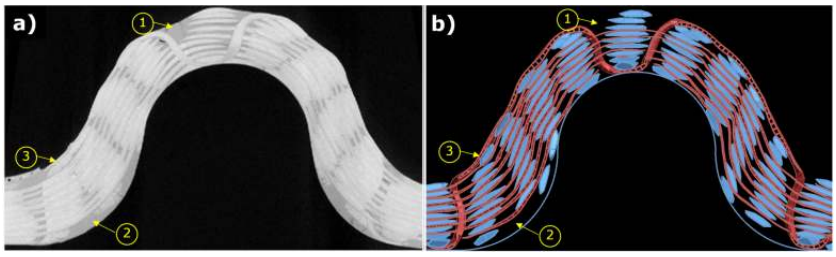

Figure 19*. Comparison between proposed model and experimental results: a) CT scan, b) Simulation.*

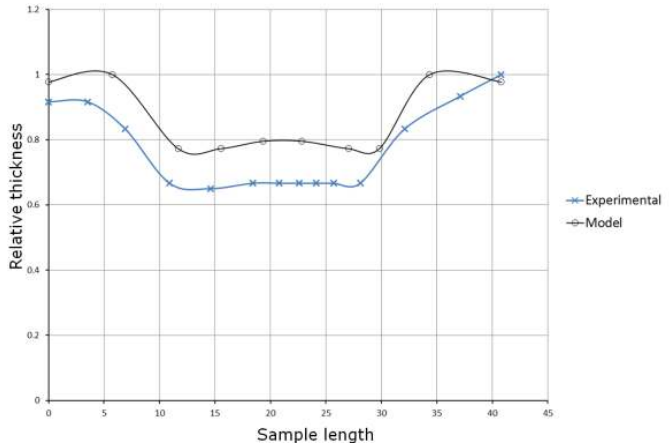

Figure 20. *Predicted thickness variation along the sample length in comparison to the experimental results.*

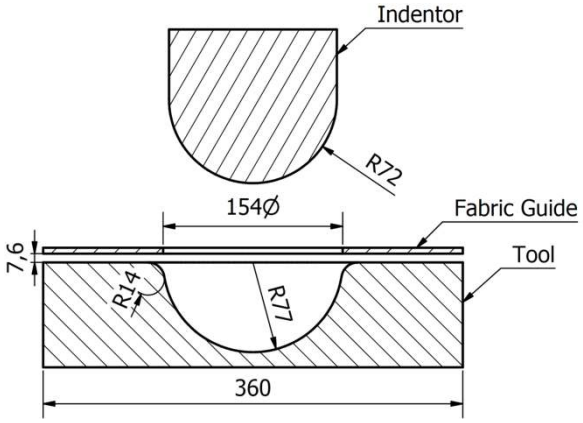

Figure 21*. Dome forming model setup and tool geometry.*

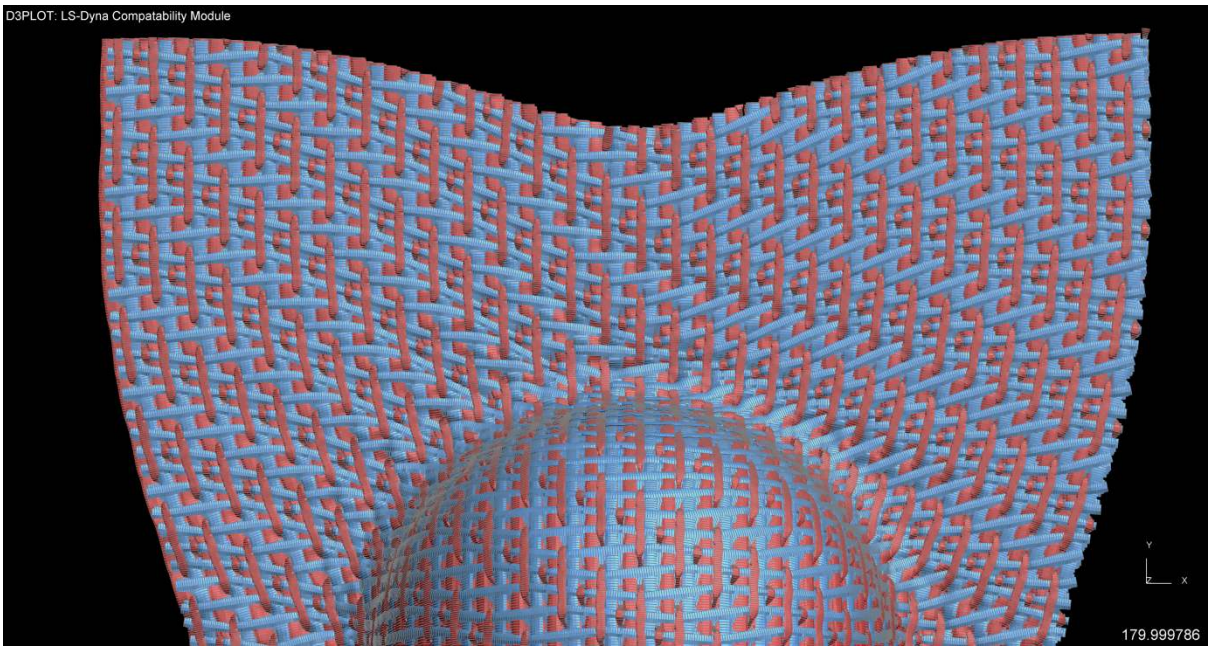

Figure 22. *Dome forming result, a top view showing one half of the model.*

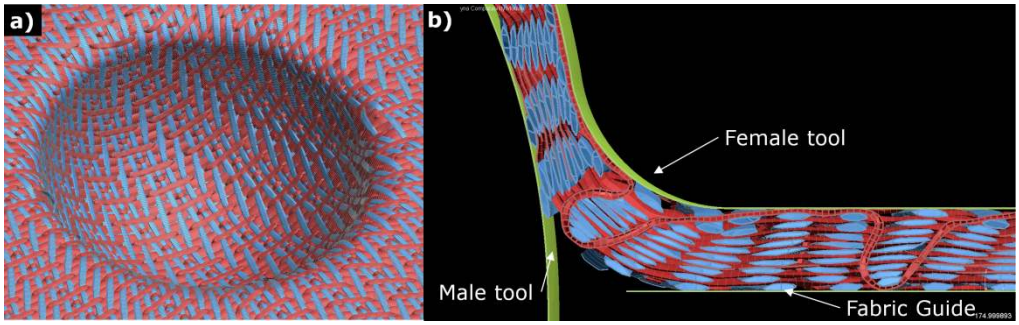

Figure 23. *Detailed dome forming results: a) close-up view of the dome inside, b) close-up cut section in the fabric at dome base showing the transition from compacted to uncompacted areas of fabric.*